RSC Advances

PAPER

View Article Online
View Journal | View Issue

Cite this: *RSC Adv.*, 2020, **10**, 12511

Effect of polyethylene glycol on crystal growth and photocatalytic activity of anatase TiO_2 single crystals

Yeshuo Dong *[a] and Fanjun Meng[b]

Received 25th February 2020
Accepted 20th March 2020

DOI: 10.1039/d0ra01796e

rsc.li/rsc-advances

In order to evaluate the effect of polyethylene glycol (PEG) on the growth of TiO_2 crystals, anatase TiO_2 crystals with different morphologies and structures were synthesized by controlling the content and type of PEG in a solvothermal system. Then, their morphology and structure were characterized by X-ray diffraction (XRD), X-ray photoelectron spectroscopy (XPS), scanning electron microscopy (SEM) and transmission electron microscopy (TEM). Characterization results show that hydrofluoric acid can promote the formation of high activity (001) facets. Experiments on the effect of PEG on crystal growth show that the low molecular weight PEG (PEG400) can accelerate crystal differentiation and relieve the agglomeration of crystals in the presence of hydrofluoric acid. Besides, according to the experimental results, we found that PEG400 can reduce the agglomeration size and number of TiO_2 polycrystalline particles. Research on the photocatalytic activity proposed that the independence of single crystal and the integrity of (001) facets are the critical factors in advanced oxidation reaction. The resultant anatase TiO_2 single crystals could produce more hydroxyl radicals (·OH) in the photocatalytic system, which exhibited remarkable photocatalytic performance for the degradation of Acid Red B.

1. Introduction

As is known to all, anatase TiO_2 has been widely used in environmental pollution control, solar cells, H_2-production, photovoltaic power generation and sensor design.[1–5] However, the application of anatase TiO_2 in the above-mentioned fields often depends on the crystal structure,[6,7] the activity of crystal plane and the specific morphology.[8–10] Therefore, the study on the atomic structure and lattice properties of TiO_2 crystal plane is the key to improve the physical and chemical properties of the material.[11–14] Moreover, for the study of the synthesis process of TiO_2, the exposure of equilibrium and stable highly active crystal facets is the key to determine the surface properties and activity of the single crystal.[15–17]

Both theoretical and experimental studies found that the (001) facets in equilibrium and stable states has a very high photocatalytic activity.[18–20] However, most anatase TiO_2 crystals are dominated by the thermodynamically stable (101) facets (more than 94%, according to the Wulff construction[21]), rather than the much more reactive (001) facets.[22] This is because the surface energy of the (001), (100) and (101) facets of anatase TiO_2 are 0.90 J m^{-2}; 0.53 J m^{-2} and 0.44 J m^{-2}, respectively. The traditional synthesis process of anatase TiO_2 always follows the principle of minimum energy, which makes the surface energy of all crystal facets of anatase TiO_2 always tends to be minimized.[23,24] In 2008, the anatase TiO_2 single crystals were synthesized with a large percentage (47%) of reactive (001) facets using hydrofluoric acid as a morphology controlling agent.[25] Then, on the basis of the above results, researchers at home and abroad began to study anatase TiO_2 single crystals more extensively and deeply, and many single crystals with different structures and morphologies were prepared.[26–29] At the same time, the research of crystal plane effect and charge motion has also been carried out, and many research results have been obtained.[30,31] The results show that the (001) facets and (101) facets of the excited state anatase TiO_2 single crystal have different electron density, and the photoelectrons tend to move from (001) to (101) facets.[32,33] As a result, a large number of holes are produced on (001) facets, and a large number of electrons are enriched on (101) facets. The study on the surface energy of crystal shows that the surface energy of (001) facets is twice as much as that of (101) facets, and the difference of energy level leads to the crystal surface effect, which promotes the movement of electric charge.[21,34,35] Besides, some studies have proposed the theory of surface heterojunction by calculating the energy level of the crystal plane band gap of single crystals.[36,37] All in all, the high activity of the single crystal depends on the synergistic effect of the (001) and (101) facets.

However, during the synthesis of TiO_2 single crystals, the characteristics of crystal agglomeration have always been a difficult problem for researchers.[38,39] The aggregation effect

[a]*School of Environmental and Municipal Engineering, Qingdao University of Technology, Qingdao, 266033, China. E-mail: dysh_1127@aliyun.com*
[b]*College of Chemistry, Chemical Engineering and Materials Science, Shandong Normal University, Jinan, 250014, China*

seriously hinders the regular growth of the crystal facets and destroys the energy level structure of the crystal plane, thus affecting the overall catalytic activity.[40,41] Therefore, in the improved synthesis of single crystals, dispersants (such as surfactant and alcohols) are often added to increase the dispersion and independence of the crystal.[42,43] To sum up, it is necessary to study the synthesis of anatase TiO_2 single crystal with independent characteristics.

Based on the above purposes, the polyethylene glycol (PEG) was chosen as a dispersant in this work. And, anatase TiO_2 crystals with different morphologies and structures were synthesized under the action of hydrofluoric acid and polyethylene glycol. The effect of polyethylene glycol on crystal growth was studied by characterization of microstructure and morphology of TiO_2 crystals. This study provides a reference for the fine synthesis of anatase TiO_2 single crystal. Moreover, in order to evaluate the photocatalytic performance of the resultant anatase TiO_2 crystals, the photocatalytic oxidation properties for heterogeneous photocatalytic reaction were monitored by terephthalic acid method and photocatalytic degradation of Acid Red B.

2. Experimental methods

2.1 Synthesis and characterization of materials

The anatase TiO_2 crystals with different morphologies were synthesized through a solvothermal route. In this work, hydrofluoric acid and polyethylene glycol were used as the crystal plane controlling agent and crystal dispersant, respectively. Titanium tetrafluoride (TiF_4; Sigma-Aldrich) was dissolved in hydrochloric acid solution under vigorous stirring to give a concentration of 0.01 mol L^{-1} with the pH value changed to 1.5. TiF_4 solution (0.01 mol L^{-1}), hydrofluoric acid (HF, 40 wt%) and polyethylene glycol (PEG) were added into a 100 mL Teflon-lined stainless steel autoclave. The autoclave was kept at 150 °C for 6–12 h in an electric oven. After reaction, the anatase TiO_2 crystals were harvested by centrifugation, cleaning and drying. The surface fluorine of the samples were removed through a heat treatment process at 500 °C for 90 min. Then, the samples were cooled to room temperature for further activity experiments and characterization.

The morphology and crystal structure of the as-synthesized anatase TiO_2 crystals were investigated by X-ray spectroscopy (XRD, Bruker D8 Advance), scanning electron microscopy (SEM, JEOLJSM6400F) and transmission electron microscopy (TEM, JEM-2100, Japan). The N_2-adsorption and desorption of the samples were measured by specific surface area analyzer (F-Sorb 3400). Specific surface areas were calculated according to Brunauer–Emmett–Teller (BET) equation. X-ray photoelectron spectroscopy (XPS) measurements were done by a Kratos AXIS Ultra DLD XPS system. All the binding energies were referenced to the C 1s peak (285.0 eV) arising from adventitious carbon.

2.2 Photocatalytic oxidation properties measurement

2.2.1. Hydroxyl radicals (˙OH) measurement. As we all know, the hydroxyl radicals (˙OH) has very high oxidation potential (2.80 eV) and strong oxidation ability.[44,45] It can react quickly with most organic pollutants and oxidize the harmful substances to CO_2, H_2O or mineral salts without selectivity, which is often used in the treatment of refractory organic wastewater. The photocatalytic oxidation properties for heterogeneous photocatalytic reaction of the resultant anatase TiO_2 crystals were monitored by measuring the formation of active hydroxyl radicals (˙OH), which are considered as the most important oxidative species in photocatalysis reactions. Terephthalic acid (TA) was used as a fluorescence probe because it can react with ˙OH in basic solution to generate 2-hydroxy terephthalic acid (TAOH), which emits the unique fluorescence signal with the spectrum peak around 426 nm (eqn (1)).

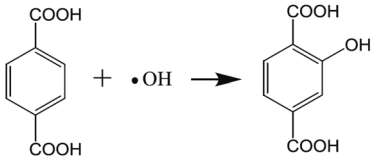

(1)

The resultant TiO_2 photocatalyst samples were suspended in 50 mL of aqueous solution containing 0.05 mol L^{-1} NaOH and 5.0 mmol L^{-1} terephthalic acid. A 350 W UV-light lamp (illumination intensity: 5260 μW cm^{-2}) was employed to provide a UV-light source. 5.0 mL of solution was taken out, and the TiO_2 was separated from the solution by a centrifugation method. The remaining clear liquid was used for fluorescence spectrum measurements. The employed excitation light in recording fluorescence spectra is 320 nm.[46]

2.2.2. Photocatalytic degradation of Acid Red B. In this work, we evaluated the photocatalytic oxidation properties of the resultant TiO_2 photocatalyst samples by photodegradation experiments of Acid Red B (50 mg L^{-1}, pH = 3). A 350 W UV-light lamp (illumination intensity: 5260 μW cm^{-2}) was positioned within the central part of the photoreactor and cooling water was circulated through a pyrex jacket surrounding the photoreactor. An UV-vis absorption spectrophotometer (UV-2500, Shimadzu, Japan) was used to determine the absorbance of oxidation products.

3. Results and discussion

3.1 Characterization

For the synthesis of anatase TiO_2 single crystals, hydrofluoric acid was used as a crystal plane controlling agent. Hydrofluoric acid was believed to have dual roles here: to retard hydrolysis of the titanium precursor and reduce surface energy to promote the isotropic growth along the [010] and [100] axes.[47,48] At the beginning of this study, the effect of hydrofluoric acid on crystal plane was studied. As shown in Fig. 1a, a control experiment for the synthesis of spherical TiO_2 polycrystalline without HF was carried out. It can be seen that only resembling spherical TiO_2 polycrystalline particles were formed, and there is no complete (001) facets (Fig. 1a2). In contrast, as shown in Fig. 1b1 and b2, anatase TiO_2 single crystals could be synthesized with hydrofluoric acid as a crystal plane controlling agent. From the

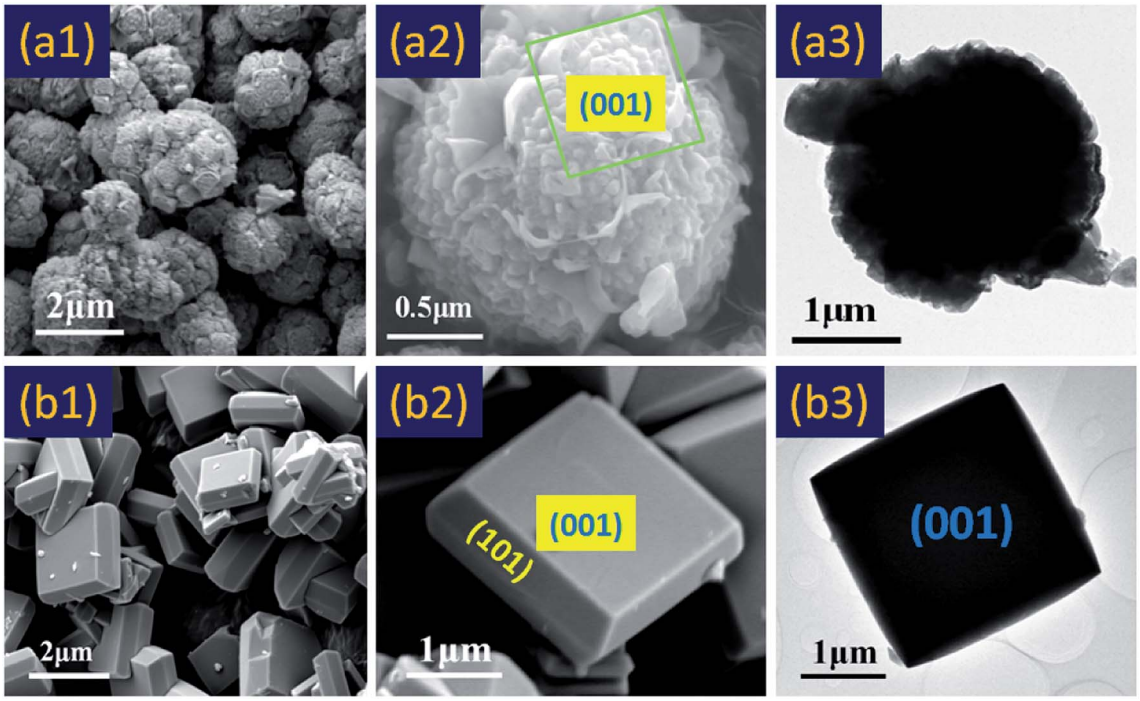

Fig. 1 Microstructure and morphology of anatase TiO_2 crystals. (a1), (a2) and (a3), SEM and TEM images of typical spherical TiO_2 polycrystalline particles (without HF). (b1), (b2) and (b3), SEM and TEM images of typical anatase TiO_2 single crystals (with HF).

symmetries of the well-faceted crystal structure of the single crystals, the two flat square surfaces are identified as (001) facets while the other eight isosceles trapezoidal surfaces are (101) facets.[25] The corresponding TEM images was shown in (Fig. 1a3) and (Fig. 1b3). As we all know, most anatase TiO_2 crystals are dominated by the thermodynamically stable (101) facets (more than 94%, according to the Wulff construction[21]), rather than the much more reactive (001) facets.[36] And the surface energy of (001; 0.90 J m^{-2}) is higher than that of (101; 0.44 J m^{-2}). Therefore, according to the principle of minimum energy of the crystal plane, the highly active (001) facets will gradually disappear during the growth of the crystal. This results in a large number of broken (001) facets on the surface of spherical TiO_2 polycrystalline particles. In view of this phenomenon, we discussed a plausible mechanism to study the reason of broken (001) facets. In an acidic environment, the TiO_2 surface is very easy to be hydroxylation under the hydrothermal conditions.[49] On the crystal surfaces, Ti atoms exist in three states: $TiOH^{2+}$, TiO^-, TiOH; as shown in the formula eqn (2) and (3).

$$\equiv Ti\text{–}OH_2^+ \rightarrow \equiv Ti\text{–}OH + H^+ \quad (2)$$

$$\equiv Ti\text{–}OH \rightarrow \equiv TiO^- + H^+ \quad (3)$$

$$\equiv Ti\text{–}OH + HF \rightarrow \equiv Ti\text{–}F + H_2O \quad (4)$$

with the prolonging of reaction time, TiOH is replaced by Ti–F through ligand exchange of hydroxyl (–OH) on the crystal surfaces and F ions (eqn (4)). With the further being replaced of surface hydroxyl groups, Ti atoms will eventually be dissolved in the system with the form of the complexes (TiF_6^{2-}).[50] This form of TiF_6^{2-} leads to the corrosion of the single crystal surface. Because of the binding effect of the sub-layer Ti atoms on the hydroxyl group, this substitution of Ti–F is easier to occur in (001) facets.[51] Therefore, it can be found that the (001) facets will be easy to be broken.

To explore the effects of polyethylene glycol (PEG) on crystal growth, a comparative experiment was designed. As shown in Fig. 2a, in the absence of hydrofluoric acid, PEG does not promote crystal differentiation. In contrast, the high molecular weight PEG (PEG4000) can interfere with the normal growth of crystals and is not conducive to the synthesis of crystals (Fig. 2a1). And, the low molecular weight PEG (PEG400) could decreases the size of spherical TiO_2 polycrystalline and increases their dispersibility (Fig. 2a3). However, in the presence of hydrofluoric acid, the low molecular weight PEG (PEG400) could promote crystal differentiation and relieve the agglomeration of crystals (Fig. 2b3). In the meantime, the experimental results show that the PEG4000 was not conducive to the crystal differentiation, and will lead to the formation of agglomerated TiO_2 single crystals (Fig. 2b1). This may be due to the crystallization of the high molecular weight PEG. Moreover, in order to further explore the effect of PEG on crystal growth, a validation experiment was designed. The results of previous experiments show that PEG400 has a good dispersibility, therefore, in this experiment, we take PEG400 as the object of study. As shown in Fig. 3, we identified two synthetic routes (R1 and R2) by regulating the addition of PEG400. Compared with Fig. 3a1 and b1, the morphology and structure of TiO_2 produced by R1 and R2 were completely different after 8 hours of reaction.

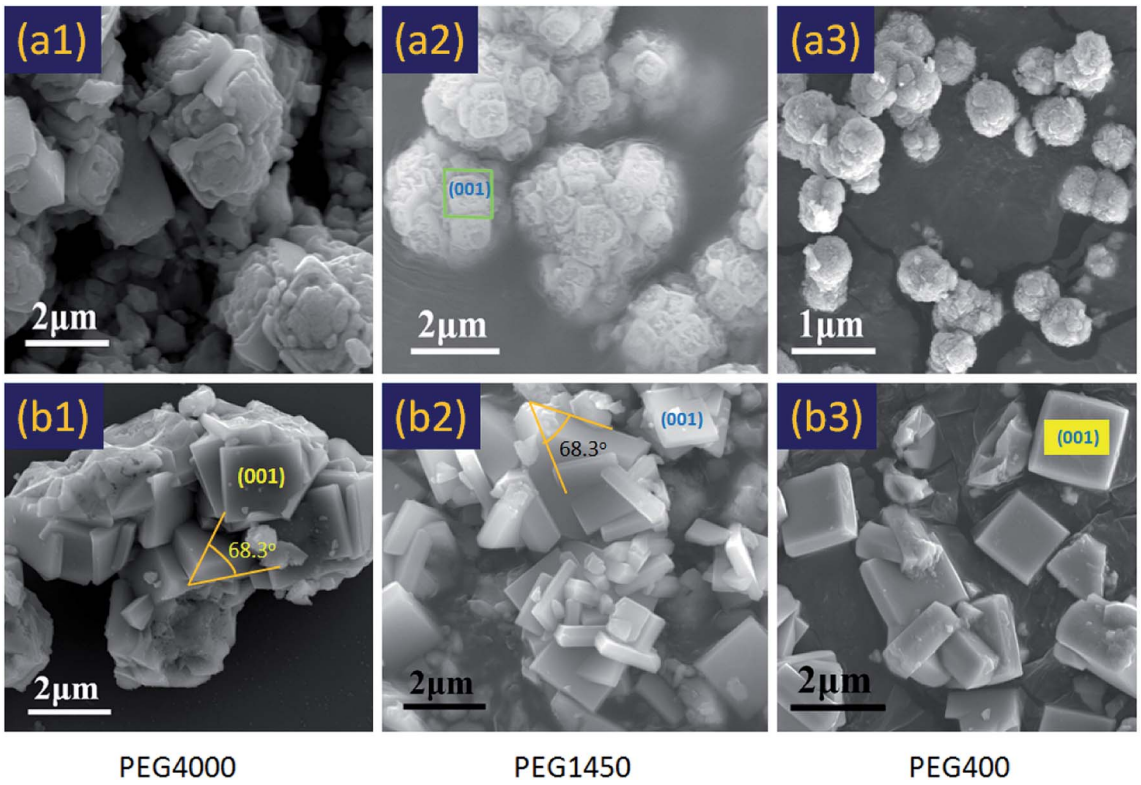

Fig. 2 Microstructure and morphology of TiO_2 crystals synthesized with different type of PEG. (a1)–(a3), SEM images of spherical TiO_2 polycrystalline particles (without HF). (b1)–(b3), SEM images of anatase TiO_2 single crystals (with HF).

As show in Fig. 3a1, it can be clearly seen that the (001) facets exposed square TiO_2 single crystal with good dispersion appears in the synthesis system. In contrast, the square TiO_2 single crystal with (001) facets exposed also appear in Fig. 3b1, but these crystals are agglomerates in appearance. The appearance of this phenomenon lays a foundation for the formation of the final morphology of single crystal. As show in Fig. 3a2 and b2, both the (101) facets and the interfacial angle (68.3°) are

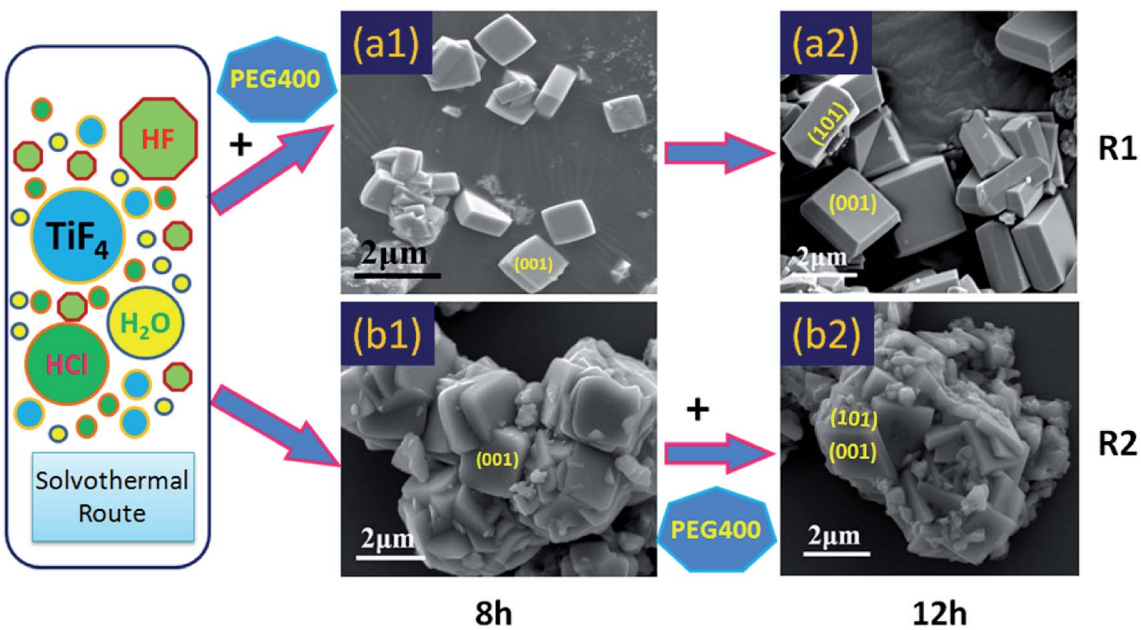

Fig. 3 The morphology of anatase TiO_2 single crystals synthesized with different reaction time: 8 h, 12 h. (a1) and (a2) Add PEG400 at the beginning of the reaction. (b1) and (b2) Add PEG400 after reaction 8 h.

generated on this basis. In summary, the low molecular weight PEG (PEG400) is believed to accelerate crystal differentiation and relieve the agglomeration of crystals in the presence of hydrofluoric acid. And, the high molecular weight PEG (PEG4000) is not beneficial to crystal growth.

In this paper, the crystallographic structure of the resultant TiO_2 crystals have been confirmed by X-ray diffraction (XRD), and the diffraction pattern in Fig. 4 clearly indicates that the samples are anatase phase (JCPDS Card no. 21-1272).[26] This means that the crystal morphology does not affect the crystal phase under certain reaction conditions. However, the diffraction peaks of anatase TiO_2 single crystals were stronger and narrower than those of the other two TiO_2 crystals. It means that the crystallinity of the anatase TiO_2 single crystals were better and higher than that of other samples. The XPS survey spectra of the as-synthesized TiO_2 samples were shown in Fig. 5. It can be seen that both anatase TiO_2 single crystals and agglomerated TiO_2 single crystals only contains Ti, O and C elements after fluorine removed, with sharp photoelectron peaks appearing at binding energies of 458 (Ti 2p), 531 (O 1s) and 285 eV (C 1s), respectively.[52] The C 1s peak is attributed to the adventitious hydrocarbon from XPS instrument itself. Besides, according to the synthesis mechanism of TiO_2 single crystal, the Ti–F species will be present on the surface of the crystal before defluorinated. So, a photoelectron peak at 684.0 eV (F 1s) will be found in the survey spectrum of fluorinated TiO_2 single crystals. However, as shown in Fig. 5, the fluorine on the surfaces of the crystals could can easily be removed by heating at 500 °C for 90 min, without changing their crystal structure and morphology. The N_2 adsorption–desorption isotherm and pore size distribution of the TiO_2 samples were shown in Fig. 6. The adsorption isotherm of the anatase TiO_2 single crystals belong to IV and H3 hysteresis loop (IUPAC), suggesting narrow slit-shaped pores that are generally associated with plate-like particles, which agrees well with their plate-like morphology.[53] And the existing narrow slit-shaped pores (or the generation of hysteresis loops) are from the aggregation of single crystals. Additionally, it can be found that the pore diameter and pore volume calculated with a BJH method was about 3.5 nm and 0.04 $cm^3\ g^{-1}$, respectively. And the specific surface area of the anatase TiO_2 single crystals calculated with the Brunauer–Emmett–Teller (BET) equation was 5.78 $m^2\ g^{-1}$.

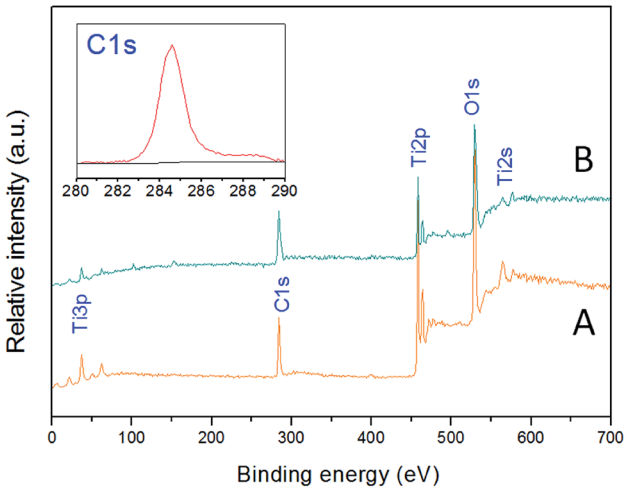

Fig. 5 XPS survey spectra of the as-synthesized anatase TiO_2 single crystals. (A) Anatase TiO_2 single crystals. (B) Agglomerated TiO_2 single crystals.

3.2 Photocatalytic oxidation properties measurement

For the hydroxyl radicals (˙OH) measurement, the capability of forming ˙OH of anatase TiO_2 single crystals; agglomerated TiO_2 single crystals and spherical TiO_2 polycrystalline was examined in this work. As shown in Fig. 7A, significant fluorescence spectra associated with TAOH was generated. The anatase TiO_2 single crystals with complete single crystal morphology and (001) facets could generate more ˙OH with the stronger

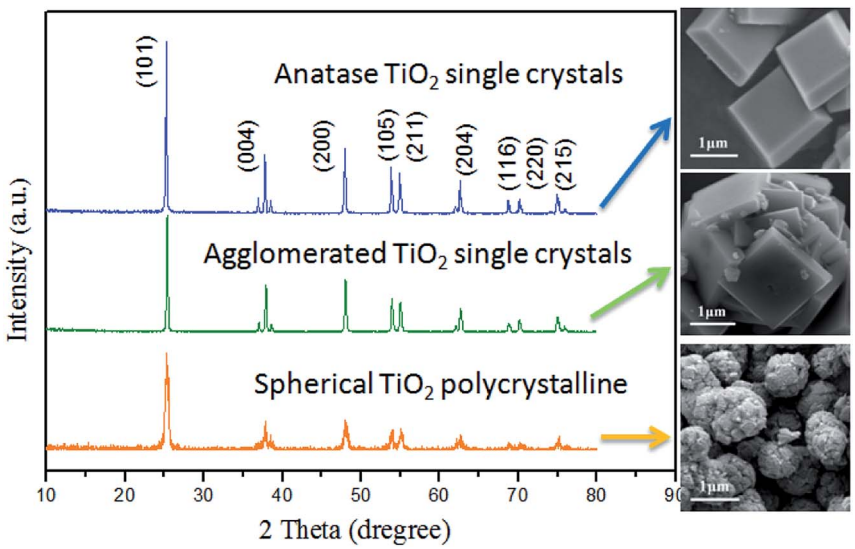

Fig. 4 XRD patterns of the resultant TiO_2 crystals samples.

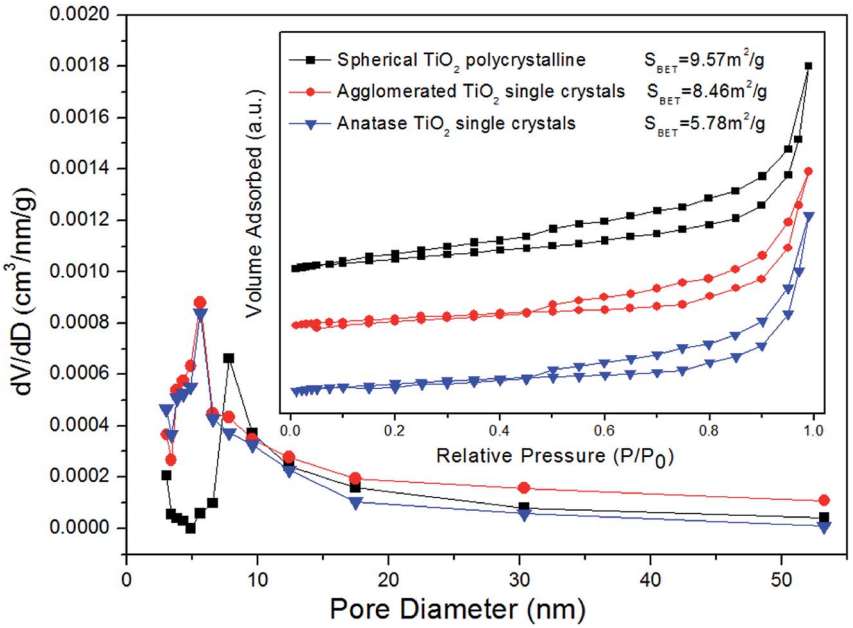

Fig. 6 N_2 adsorption–desorption isotherm (inset) and pore size distribution of the TiO_2 samples.

oxidation ability. From the analysis of Fig. 7A and B, we find that the generation of hydroxyl radical on anatase TiO_2 single crystal is a short-time explosion. After 30 minutes of reaction, the yield of hydroxyl radical basically reached the peak. The results clearly demonstrate the exposure area of (001) facets is the key to the generation of hydroxyl radical. Moreover, the normalized concentration of $^{\bullet}OH$ generated from anatase TiO_2 single crystals is higher than that of the other two TiO_2 samples. It is also proposed that the simultaneous exposure of the (001) and (101) facets could facilitate charge separation due to the difference in the energy levels of different crystal facets. Therefore, we can infer that the anatase TiO_2 single crystals has a complete crystal structure (including (001) and (101) facets), which makes the surface charge move more rapidly and promotes the separation of photoelectron holes.

Owing to the result of hydroxyl radicals ($^{\bullet}OH$) measurement the complete morphology of the anatase TiO_2 single crystal with (001) and (101) facets, the charge transport will be faster, and this can help to promote the separation of photogenerated electrons and holes, thereby greatly improving the photocatalytic activities.[54] To confirm this, we performed photocatalytic degradation of Acid Red B as a probe reaction.

Fig. 8 shows the photocatalytic degradation efficiency of Acid Red B (characteristic adsorption peak of Acid Red B at 515 nm). In order to study the photocatalytic activity of TiO_2 on Acid Red B more scientifically, we conducted a comparative experiment without any TiO_2 (Fig. 8B). The results show that the Acid Red B could undergo photolysis under ultraviolet light, which leads to decolorization. As shown in Fig. 8B (darkness reaction), the removal rate of Acid Red B is proportional to the specific surface area.[55] This is mainly due to the larger specific surface area is more conducive to the adsorption of dyes. However, Fig. 8B also shows that the photocatalytic activity is inversely proportional to the specific surface area during the photocatalytic reaction.

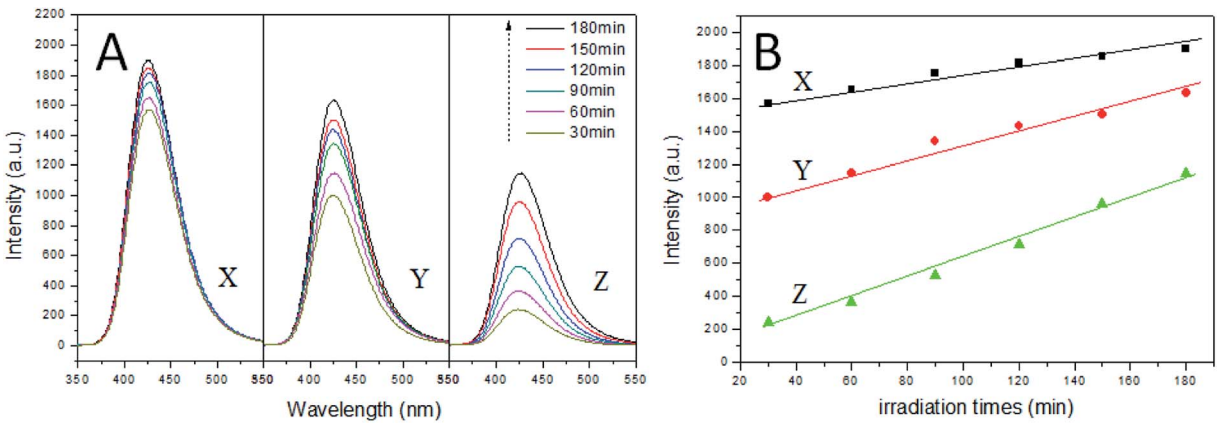

Fig. 7 (A) Fluorescence spectra of 5 mmol L^{-1} terephthalic acid after different irradiation times. (B) Comparison on photocatalytic oxidation activity with different photocatalyst. (X) Anatase TiO_2 single crystals; (Y) agglomerated TiO_2 single crystals; (Z) spherical TiO_2 polycrystalline.

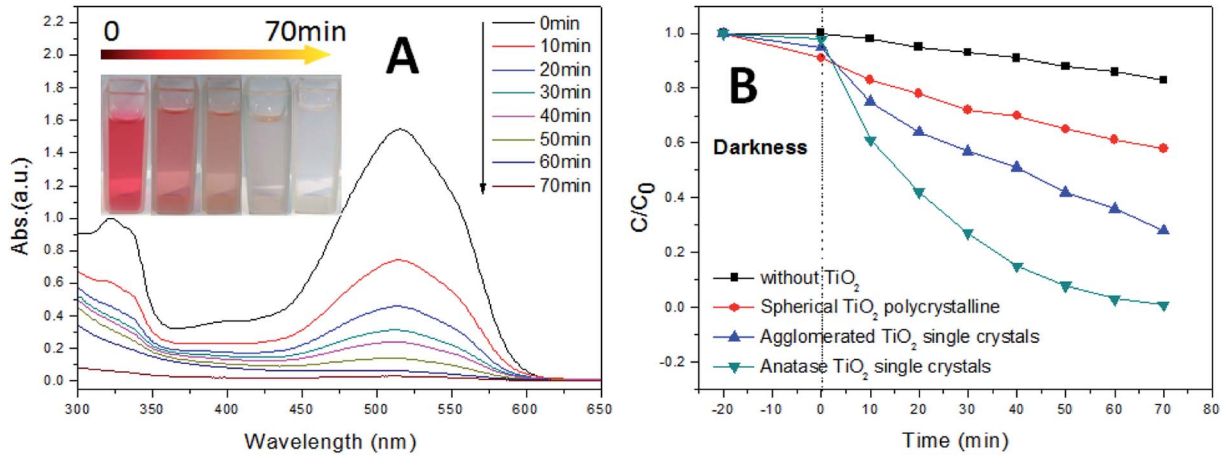

Fig. 8 (A) Acid Red B degradation *versus* irradiation time in the presence of anatase TiO_2 single crystals. (B) Comparison on photocatalytic oxidation activity with different photocatalyst. (C) The mechanism of photocatalytic oxidation Acid Red B on anatase TiO_2 single crystals.

The experimental results show that the effect of specific surface area on photocatalytic activity is not decisive. On the contrary, the complete crystal plane structure is the key to the high activity of photocatalysis. Therefore, the anatase TiO_2 single crystals showed remarkably higher efficiencies in the photocatalytic degradation of Acid Red B than the other corresponding TiO_2 crystals. This is due to the existence of the (001) and (101) facets can form an interface effect, which accelerates the transfer rate of photoelectron holes on the crystal surface. Furthermore, it is shown that the photoelectron of excited TiO_2 tends to move from (001) to (101) facets, therefore, the accumulation of photogenic holes on the (001) surface will lead to strong oxidation. Significantly, as shown in the SEM images of the agglomerated TiO_2 single crystals, because of the agglomeration, the exposure ratio of (001) and (101) facets is very low, which severely limits the photocatalytic activity.

4. Conclusions

In this work, the effect mechanism of polyethylene glycol on crystal growth was studied. For this purpose, anatase TiO_2 crystals with different morphologies and structures were synthesized. Characterization results show that anatase TiO_2 single crystals with high activity (001) facets could be synthesized by using hydrofluoric acid as the crystal plane controlling agent. Experiments on the effect of polyethylene glycol on crystal growth show that the low molecular weight PEG (PEG400) can accelerate crystal differentiation and relieve the agglomeration of crystals in the presence of hydrofluoric acid. Besides, the PEG400 can also reduce the agglomeration size and number of TiO_2 polycrystalline particles. Research on the photocatalytic activity proposed that the independence of single crystal and the integrity of (001) facets are the critical factors in advanced oxidation reaction. The resultant anatase TiO_2 single crystals could produce more hydroxyl radicals ($^{\bullet}OH$) due to the interface effect between (001) and (101) facets, which exhibited remarkable photocatalytic performance for the degradation of Acid Red B.

Conflicts of interest

There are no conflicts to declare.

References

1 X. Li, J. G. Yu and M. Jaroniec, *Chem. Soc. Rev.*, 2016, **45**, 2603–2636.
2 A. Zarkadoulas, E. Koutsouri, C. Kefalidi and C. A. Mitsopoulou, *Coord. Chem. Rev.*, 2015, **304**, 55–72.
3 M. Pastore, T. Etienne and F. De Angelis, *J. Mater. Chem. C*, 2016, **4**, 4346–4373.
4 M. N. Chong, B. Jin, C. W. K. Chow and C. Saint, *Water Res.*, 2010, **44**, 2997–3027.
5 P.-Y. Hsieh, Y.-H. Chiu, T.-H. Lai, M.-J. Fang, Y.-T. Wang and Y.-J. Hsu, *ACS Appl. Mater. Interfaces*, 2019, **11**, 3006–3015.
6 Y.-H. Chiu, T.-H. Lai, C.-Y. Chen, P.-Y. Hsieh, K. Ozasa, M. Niinomi, K. Okada, T.-F. M. Chang, N. Matsushita, M. Sone and Y.-J. Hsu, *ACS Appl. Mater. Interfaces*, 2018, **10**, 22997–23008.
7 Y.-S. Chang, M. Choi, M. Baek, P.-Y. Hsieh, K. Yong and Y.-J. Hsu, *Appl. Catal., B*, 2018, **225**, 379–385.
8 A. Meng, J. Zhang, D. Xu, B. Cheng and J. Yu, *Appl. Catal., B*, 2016, **198**, 286–294.
9 X. H. Lu, G. M. Wang, T. Zhai, M. H. Yu, J. Y. Gan, Y. X. Tong and Y. Li, *Nano Lett.*, 2012, **12**, 1690–1696.
10 Y.-H. Chiu, T.-H. Lai, M.-Y. Kuo, P.-Y. Hsieh and Y.-J. Hsu, *APL Mater.*, 2019, **7**, 080901.
11 W. X. Huang, *Acc. Chem. Res.*, 2016, **49**, 520–527.
12 J. G. Yu, L. F. Qi and M. Jaroniec, *J. Phys. Chem. C*, 2010, **114**, 13118–13125.
13 Y.-H. Chiu, T.-F. M. Chang, C.-Y. Chen, M. Sone and Y.-J. Hsu, *Catalysts*, 2019, **9**, 430.
14 J.-M. Li, Y.-T. Wang and Y.-J. Hsu, *Electrochim. Acta*, 2018, **267**, 141–149.
15 Y. W. Jun, M. F. Casula, J. H. Sim, S. Y. Kim, J. Cheon and A. P. Alivisatos, *J. Am. Chem. Soc.*, 2003, **125**, 15981–15985.

16 E. J. W. Crossland, N. Noel, V. Sivaram, T. Leijtens, J. A. Alexander-Webber and H. J. Snaith, *Nature*, 2013, **495**, 215–219.
17 T.-F. M. Chang, W.-H. Lin, C.-Y. Chen, Y.-J. Hsu and M. Sone, *MRS Commun.*, 2017, **7**, 189–192.
18 Y. Bai, P. Y. Luo, P. Q. Wang and J. Y. Liu, *Catal. Commun.*, 2013, **37**, 45–49.
19 S. L. Chen, D. Li, Y. X. Liu and W. X. Huang, *J. Catal.*, 2016, **341**, 126–135.
20 X. Q. Gong and A. Selloni, *J. Phys. Chem. B*, 2005, **109**, 19560–19562.
21 M. Lazzeri, A. Vittadini and A. Selloni, *Phys. Rev. B: Condens. Matter Mater. Phys.*, 2001, **63**(15), 155409.
22 H. M. Zhang, Y. Wang, P. R. Liu, Y. H. Han, X. D. Yao, J. Zou, H. M. Cheng and H. J. Zhao, *ACS Appl. Mater. Interfaces*, 2011, **3**, 2472–2478.
23 X. Y. Ma, Z. G. Chen, S. B. Hartono, H. B. Jiang, J. Zou, S. Z. Qiao and H. G. Yang, *Chem. Commun.*, 2010, **46**, 6608–6610.
24 Y. Q. Dai, C. M. Cobley, J. Zeng, Y. M. Sun and Y. N. Xia, *Nano Lett.*, 2009, **9**, 2455–2459.
25 H. G. Yang, C. H. Sun, S. Z. Qiao, J. Zou, G. Liu, S. C. Smith, H. M. Cheng and G. Q. Lu, *Nature*, 2008, **453**, 638–641.
26 H. G. Yang, G. Liu, S. Z. Qiao, C. H. Sun, Y. G. Jin, S. C. Smith, J. Zou, H. M. Cheng and G. Q. Lu, *J. Am. Chem. Soc.*, 2009, **131**, 4078–4083.
27 T. Taguchi, Y. Saito, K. Sarukawa, T. Ohno and M. Matsumura, *New J. Chem.*, 2003, **27**, 1304–1306.
28 T. Nagata, K. Kobashi, Y. Yamashita, H. Yoshikawa, C. Paulsamy, Y. Suzuki, T. Nabatame, A. Ogura and T. Chikyow, *Thin Solid Films*, 2015, **591**, 105–110.
29 M. Liu, L. Y. Piao, W. M. Lu, S. T. Ju, L. Zhao, C. L. Zhou, H. L. Li and W. J. Wang, *Nanoscale*, 2010, **2**, 1115–1117.
30 G. Liu, H. G. Yang, J. Pan, Y. Q. Yang, G. Q. Lu and H. M. Cheng, *Chem. Rev.*, 2014, **114**, 9559–9612.
31 Q. Kuang, X. Wang, Z. Y. Jiang, Z. X. Xie and L. S. Zheng, *Acc. Chem. Res.*, 2014, **47**, 308–318.
32 T. Bredow and K. Jug, *J. Phys. Chem.*, 1995, **99**, 285–291.
33 M. M. Maitani, K. Tanaka, D. Mochizuki and Y. Wada, *J. Phys. Chem. Lett.*, 2011, **2**, 2655–2659.
34 T. Tachikawa, S. Yamashita and T. Majima, *J. Am. Chem. Soc.*, 2011, **133**, 7197–7204.
35 M. D'Arienzo, J. Carbajo, A. Bahamonde, M. Crippa, S. Polizzi, R. Scotti, L. Wahba and F. Morazzoni, *J. Am. Chem. Soc.*, 2011, **133**, 17652–17661.
36 J. G. Yu, J. X. Low, W. Xiao, P. Zhou and M. Jaroniec, *J. Am. Chem. Soc.*, 2014, **136**, 8839–8842.
37 M. Batzill, *Energy Environ. Sci.*, 2011, **4**, 3275–3286.
38 M. G. Xu, P. Ruan, H. X. Xie, A. Yu and X. F. Zhou, *ACS Sustainable Chem. Eng.*, 2014, **2**, 621–628.
39 Y. Dong and X. Fei, *Mater. Technol.*, 2020, **35**, 102–111.
40 Y. Zhang, Y. Chen, Y. W. Zhao and N. Xiang, *Mater. Technol.*, 2018, **33**, 592–602.
41 H. Liu, D. R. Li, X. L. Yang and H. F. Li, *Mater. Technol.*, 2019, **34**, 192–203.
42 R. K. Mahajan, J. Chawla, K. K. Vohra and V. K. Aswal, *J. Appl. Polym. Sci.*, 2010, **117**, 3038–3046.
43 J.-M. Li, C.-W. Tsao, M.-J. Fang, C.-C. Chen, C.-W. Liu and Y.-J. Hsu, *ACS Appl. Nano Mater.*, 2018, **1**, 6843–6853.
44 S. S. Shinde, C. H. Bhosale and K. Y. Rajpure, *Catal. Rev.*, 2013, **55**, 79–133.
45 Y. F. Li, D. H. Xu, J. I. Oh, W. Shen, X. Li and Y. Yu, *ACS Catal.*, 2012, **2**, 391–398.
46 Y. J. Wang, Y. M. He, T. T. Li, J. Cai, M. F. Luo and L. H. Zhao, *Chem. Eng. J.*, 2012, **189**, 473–481.
47 M. Crippa, E. Callone, M. D'Arienzo, K. Muller, S. Polizzi, L. Wahba, F. Morazzoni and R. Scotti, *Appl. Catal., B*, 2011, **104**, 282–290.
48 R. L. Penn and J. F. Banfield, *Geochim. Cosmochim. Acta*, 1999, **63**, 1549–1557.
49 G. S. Wu, J. P. Wang, D. F. Thomas and A. C. Chen, *Langmuir*, 2008, **24**, 3503–3509.
50 H. G. Yang and H. C. Zeng, *Angew. Chem., Int. Ed.*, 2004, **43**, 5206–5209.
51 C. P. Sajan, S. Wageh, A. A. Al-Ghamdi, J. G. Yu and S. W. Cao, *Nano Res.*, 2016, **9**, 3–27.
52 Z. Y. Wang, K. L. Lv, G. H. Wang, K. J. Deng and D. G. Tang, *Appl. Catal., B*, 2010, **100**, 378–385.
53 G. D. Jiang, M. Wei, S. D. Yuan and Q. Chang, *Appl. Surf. Sci.*, 2016, **362**, 418–426.
54 M. Sumita, C. P. Hu and Y. Tateyama, *J. Phys. Chem. C*, 2010, **114**, 18529–18537.
55 Y.-H. Chiu and Y.-J. Hsu, *Nano Energy*, 2017, **31**, 286–295.

